An explicit time-domain finite element method for room acoustics simulations: Comparison of the performance with implicit methods

Takeshi Okuzono[a,],[1] Takumi Yoshida[a], Kimihiro Sakagami[a], Toru Otsuru[b]

[a] *Environmental Acoustic Laboratory, Department of Architecture, Graduate School of Engineering, Kobe University, 1-1, Rokkodai, Nada, Kobe 657-8501, Japan*

[b] *Department of Architecture and Mechatronics, Architecture Course, Faculty of Engineering, Oita University, 700 Dannoharu, Oita 870-1192, Japan*

Abstract

This paper presents the applicability of an explicit time-domain finite element method (TD-FEM) using a dispersion reduction technique called modified integration rules (MIR) on room acoustics simulations with a frequency-independent finite impedance boundary. First, a dispersion error analysis and a stability analysis are performed to derive the dispersion relation and the stability condition of the present explicit TD-FEM for three-dimensional room acoustics simulations with an infinite impedance boundary. Secondly, the accuracy and efficiency of the explicit TD-FEM are presented by comparing with implicit TD-FEM using MIR through room acoustics simulations in a rectangular room with infinite impedance boundaries. Thirdly, the stability condition of the explicit TD-FEM is investigated numerically in the case with finite impedance boundaries. Finally, the performance of the explicit TD-FEM in room acoustics simulations with finite impedance boundaries is demonstrated in a comparison with the implicit TD-FEM. Although the stability of the present explicit TD-FEM is dependent on the impedance values given at boundaries, the explicit TD-FEM is computationally more efficient than the implicit method from the perspective of computational time for acoustics simulations of a room with larger impedance values at boundaries.

[1] Corresponding author. Tel./fax: +81 78 803 6577.
E-mail address: okuzono@port.kobe-u.ac.jp (T. Okuzono).

Keywords: Room acoustics simulations, Time domain finite element method, Explicit method, Dispersion error, Implicit method

1. Introduction

Recently, the applicability and the practicality of the wave based acoustics simulation techniques such as finite element method (FEM), boundary element method and finite difference time domain method are gradually increasing in room acoustics design, with the rapid progress of computer technology [1]. Among them, FEM is a powerful tool for predicting a sound field in a room with complex boundary conditions. Because FEM is frequently said to be computationally expensive for room acoustics simulations, the application range is restricted to low-frequency regions in general, but the situation is changing quickly with the development of efficient methods. Dispersion reduction methods such as high order finite elements (FEs) [2, 3], Krylov subspace iterative methods [4] and parallel computation methods are examples of techniques to increase the efficiency of the FEM. Thanks to the FEM using these techniques, room acoustics simulations at high frequencies have recently become within the scope of the analysis if the volume of architectural space is relatively small [5].

The FEM can analyze a sound field in a room in both frequency and time domains [6, 7, 8, 9]. Because a time-domain FEM (TD-FEM) calculates an impulse response of a room directly in a time domain, it is attractive from the perspective of room acoustics evaluations such as the visualization, the auralization of sound fields and the calculation of room acoustical parameters. The authors have also developed some efficient TD-FEM for large-scale room acoustics simulations with many degrees of freedom (DOF), and the applicability has been presented by several room acoustics simulations such as concert halls and reverberation chambers [5, 10, 11, 12]. To analyze a sound field efficiently, the TD-FEM uses a high order FEs called hexahedral 27-node spline acoustic elements [13, 5] or low-order FEs called hexahedral 8-node elements with modified integration rules (MIR) [15] as well as the use of iterative methods [4] and parallel computation methods [14]. Here, MIR is a simple dispersion reduction technique to reduce an inherent dispersion error coming from the spatial and time discretizations of a computational domain. Although the TD-FEM is based on an implicit method, it can be considered as efficient because the large-scale linear system of equations with

a sparse matrix at each time step can solve easily using an iterative method with the good convergence property [5, 10, 11].

On the other hand, there exists an explicit TD-FEM with MIR [15], in which fourth-order accuracy with respect to the dispersion error can be obtained for the idealized case using square or cubic FEs. The explicit TD-FEM is also very attractive for realizing an efficient room acoustics simulation because it does not need a solution of a linear system of equations at each time step. With this advantage, it might be computationally more efficient than the implicit TD-FEM and might become an alternative method for room acoustics simulations. However, it has not been applied to room acoustics simulations so far, and the formulation including a dissipation term for treating an absorption at boundaries has not been presented in the literature [15], which is important for room acoustics simulations. More recently, in Ref. [16], the authors presented an explicit TD-FEM using MIR with the dissipation term for room acoustics simulations, and showed the efficiency in term of computational time over an implicit TD-FEM using MIR. However, this study was conducted in limited numerical conditions without a dispersion error analysis and a stability analysis, as a first stage of the research. Therefore, to properly use the method on room acoustics simulations, the applicability of explicit TD-FEM and the performance over implicit TD-FEM need to be examined further.

In this paper, the applicability of the present explicit TD-FEM with the dissipation term on room acoustics simulations is discussed in more detail, including the three-dimensional dispersion error analysis and the stability analysis. The purpose of this paper is to show the accuracy and efficiency of the explicit TD-FEM over the implicit TD-FEM using MIR on room acoustics simulations with a frequency-independent finite impedance boundary. To this end, we conducted theoretical and numerical investigations in a step-by-step manner. First, in Section 3, to show the basic discretization error property of explicit TD-FEM in three-dimensions, a three-dimensional dispersion error analysis is performed, in which we consider an idealized condition for theoretical analysis, which is a plane wave propagation in a free field. This section also includes the comparison of dispersion property between explicit and implicit TD-FEM. Secondly, in Section 4, the theoretical findings are confirmed in room acoustics simulations with infinite impedance boundaries by a comparison between numerical solution and analytical solution because the dispersion error analysis does not consider sound wave propagations in a closed sound field. Thirdly, for more practical problems with frequency-

independent finite impedance boundaries, the stability of explicit TD-FEM is examined numerically in Section 5. Finally, the performance of explicit TD-FEM over the implicit TD-FEM on room acoustics simulations with finite impedance boundaries is discussed in Section 6, to show the applicability. Note that numerical investigations are limited to rectangular rooms modeled by the cubic FEs because the explicit TD-FEM can achieve the fourth-order accuracy for the use of only cubic FEs.

2. Theory

2.1. Implicit TD-FEM using MIR and iterative method

We consider a closed sound field with a rigid boundary, a vibration boundary, and an impedance boundary governed by the wave equation. By introducing the FE approximations to sound pressure and weight function in the weak form derived from the wave equation, the semi-discretized matrix equation for the closed sound field is obtainable as

$$\boldsymbol{M}\ddot{\boldsymbol{p}} + c_0^2\boldsymbol{K}\boldsymbol{p} + c_0\boldsymbol{C}\dot{\boldsymbol{p}} = \boldsymbol{f}, \tag{1}$$

where $\boldsymbol{M}$, $\boldsymbol{K}$, and $\boldsymbol{C}$, respectively, denote the global mass matrix, the global stiffness matrix, and the global dissipation matrix. Further, $\boldsymbol{p}$, $\boldsymbol{f}$, c_0, respectively, denote the sound pressure vector, the external force vector, and the speed of sound. The symbols $\cdot$ and $\cdot\cdot$ respectively signify first-order and second-order derivatives with respect to time. The implicit method solves the above second-order ordinary differential equation (ODE) by using a direct time integration method. In this paper, an efficient formulation for large-scale analyses with many degree of freedom is used to solve the Eq. (1) [11]. In the formulation, a Krylov subspace iterative method called Conjugate Gradient (CG) method is used to solve the large-scale linear system of equations at each time step efficiently. Furthermore, 8-node hexahedral FEs and Newmark β method [17] are respectively used for spatial and time discretizations, with MIR. The MIR is a simple method to reduce the dispersion error, in which numerical integration points of Gauss-Legendre rule in calculations of the element stiffness matrix $\boldsymbol{k}_{\mathrm{e}}$ and the element mass matrix $\boldsymbol{m}_{\mathrm{e}}$ are modified from conventional points based on the dispersion error analysis. The modified integration points for TD-FEM with 8-node hexahedral FEs and Newmark β method are given as [15]

$$\alpha_k = \pm\sqrt{\frac{2}{3}}, \quad \alpha_m = \pm\sqrt{\frac{2}{3} + (\frac{1}{3} - 4\beta)\tau^2}, \tag{2}$$

where α_k and α_m represent the numerical integration points in $\boldsymbol{m}_{\mathrm{e}}$ and $\boldsymbol{k}_{\mathrm{e}}$, respectively. τ and β represent the courant number $c_0\Delta t/h$ and a parameter related to the accuracy and the stability in Newmark β method.

Various Newmark schemes have been used with the different values of parameter β [17, 18]. This paper uses two Newmark β methods called the constant average acceleration (CAA) method with $\beta = 1/4$ and the Fox-Goodwin (FG) method with $\beta = 1/12$. For a three-dimensional analysis using cubic FEs, the stability condition of the implicit TD-FEM used here is given as [11]

$$\Delta t_{\mathrm{crit}} \leq \frac{h}{c_0} \quad (\mathrm{CAA}), \tag{3}$$

$$\Delta t_{\mathrm{crit}} \leq \frac{h}{\sqrt{3}c_0} \quad (\mathrm{FG}), \tag{4}$$

where Δt_{crit} and h respectively represent the critical time interval and the element length of cubic FEs. The dispersion error, which is defined as the difference between the exact speed of sound c_0 and approximate speed of sound c^h, of the implicit TD-FEM with CAA for the idealized case using cubic FEs can be estimated by [11]

$$\frac{|c_0 - c^h|}{c_0} = \frac{k^4h^4}{1440}[A_1 + A_2 + A_3 + A_4], \tag{5}$$

with

$$\begin{aligned}
A_1 &= 3 - 3\tau^4 - \chi_{\mathrm{i}} \cos^2\theta \sin^2\theta, \\
A_2 &= \chi_{\mathrm{i}} \cos^2\phi \sin^2\phi \cos^2\theta \sin^2\theta, \\
A_3 &= -\chi_{\mathrm{i}} \cos^2\phi \sin^2\phi \sin^2\theta, \\
A_4 &= 9 \cos^2\phi \sin^2\phi \cos^2\theta \sin^4\theta, \\
\chi_{\mathrm{i}} &= 9 - 20\tau^4,
\end{aligned} \tag{6}$$

where k, θ and ϕ respectively represent the wave number, elevation and azimuth in a spherical coordinate system. For the implicit TD-FEM with FG, the dispersion error is [11]

$$\frac{|c_0 - c^h|}{c_0} = \frac{k^4h^4}{480}[\cos^6\phi \sin^6\theta + \sin^6\phi \sin^6\theta + \cos^6\theta - \tau^4]. \tag{7}$$

Note that only the implicit TD-FEM with FG can achieve the fourth-order accuracy even for the use of rectangular FEs.

2.2. Explicit TD-FEM using MIR

In contrast to the implicit method, the explicit TD-FEM solves a first order ODE. By introducing a diagonal mass matrix $\boldsymbol{D}$ lumped from $\boldsymbol{M}$ and a vector $\boldsymbol{v} = \dot{\boldsymbol{p}}$, the second order ODE of Eq. (1) is transformed into [15, 19]

$$\boldsymbol{D}\dot{\boldsymbol{p}} = \boldsymbol{M}\boldsymbol{v}, \tag{8}$$

$$\boldsymbol{D}\dot{\boldsymbol{v}} = \boldsymbol{f} - c_0^2\boldsymbol{K}\boldsymbol{p} - c_0\boldsymbol{C}\dot{\boldsymbol{p}}, \tag{9}$$

Discretization of $\dot{\boldsymbol{p}}$ in Eq. (8) and $\dot{\boldsymbol{v}}$ in Eq. (9) by the second-order accurate central difference and $\dot{\boldsymbol{p}}$ in Eq. (9) by the first-order accurate backward difference lead to the following explicit scheme as [16]

$$\boldsymbol{p}^n = \boldsymbol{p}^{n-1} + \Delta t\boldsymbol{D}^{-1}\boldsymbol{M}\boldsymbol{v}^{n-\frac{1}{2}}, \tag{10}$$

$$\boldsymbol{v}^{n+\frac{1}{2}} = \boldsymbol{v}^{n-\frac{1}{2}} + \Delta t\boldsymbol{D}^{-1}[\boldsymbol{f}^n - c_0^2\boldsymbol{K}\boldsymbol{p}^n - \frac{c_0}{\Delta t}\boldsymbol{C}(\boldsymbol{p}^n - \boldsymbol{p}^{n-1})], \tag{11}$$

where n represents the time step. In this formulation, a sparse matrix storage format is used for storing $\boldsymbol{M}$ and $\boldsymbol{K}$, which enhances the numerical efficiency. Further, lumped dissipation matrix is also used for $\boldsymbol{C}$ to avoid the calculation of matrix-vector products. With this treatments, two sparse matrix-vector products, $\boldsymbol{M}\boldsymbol{v}^{n-\frac{1}{2}}$ and $\boldsymbol{K}\boldsymbol{p}^n$, are the main numerical operation of this explicit TD-FEM. Note that these techniques are naturally used in the implicit method.

For this explicit TD-FEM, cubic shaped 8-node hexahedral FEs are used. The element matrix $\boldsymbol{D}$ is lumped using standard Gauss-Legendre rule. Meanwhile, element matrices of $\boldsymbol{K}$ and $\boldsymbol{M}$ are constructed using MIR where the respective modified integration points are given as [15]

$$\alpha_k = \pm\sqrt{\frac{2}{3}},\ \alpha_m = \pm\sqrt{\frac{1}{3}(4-\tau^2)}. \tag{12}$$

With the modified integration points, a fourth-order accuracy with respect to the dispersion error is achieved for the idealized case using cubic FEs in a free space. The three-dimensional dispersion relation and the stability condition are presented in the next section.

3. Dispersion error analysis

3.1. Three-dimensional dispersion relation

The three-dimensional dispersion error analysis is performed to evaluate the dispersion error of explicit TD-FEM. The analysis follows the same procedure in two-dimensions [15] using the following linear multistep form without

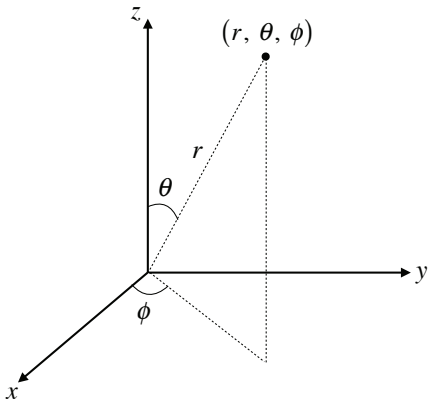

Figure 1: A spherical coordinate system, where r, θ and ϕ respectively represent distance from the origin, elevation and azimuth.

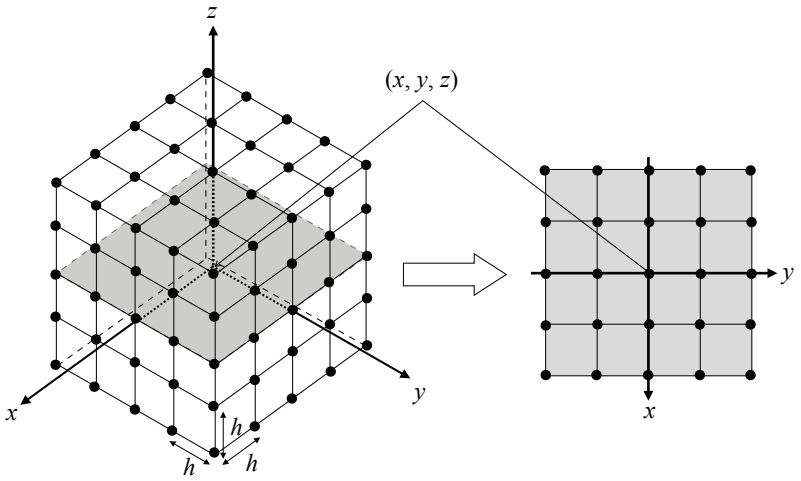

Figure 2: 125 nodes 64 cubic elements patch for dispersion error analysis in three dimensions.

source and dissipation terms, which is equivalent to Eqs (10) and (11):

$$[\boldsymbol{p}^{n+1} - 2\boldsymbol{p}^{n} + \boldsymbol{p}^{n-1}] + \Delta t^2 c_0^2 \boldsymbol{D}^{-1}\boldsymbol{M}\boldsymbol{D}^{-1}\boldsymbol{K}\boldsymbol{p}^{n} = 0. \tag{13}$$

In a spherical coordinate system (Fig. 1), the approximate plane wave $\boldsymbol{p}^n_{x,y,z}$ at time $n\Delta t$ and a location $(x,\ y,\ z)$ is given as

$$\boldsymbol{p}^n_{x,y,z} = \exp[i(k_x^h x + k_y^h y + k_z^h z - \omega^h n\Delta t)], \tag{14}$$

where $k_x^h = k^h \sin\theta\cos\phi$, $k_y^h = k^h \sin\theta\sin\phi$, $k_z^h = k^h\cos\theta$. k^h and ω^h represent the approximate wave number and the approximate angular frequency.

To evaluate the dispersion error, a region that consists of 64 FEs with an cubic shaped 8-node linear elements of size h as shown in Fig. 2 is considered. The dispersion error can be evaluated by constructing the FE equation of Eq. (13) at a center node $(x,\ y,\ z)$. The first term of Eq. (13) can be represented using Eq. (14) as

$$[\boldsymbol{p}^{n+1} - 2\boldsymbol{p}^n + \boldsymbol{p}^{n-1}] = 2(\cos\omega^h\Delta t - 1)\boldsymbol{p}^n_{x,y,z}. \tag{15}$$

The element mass matrix $\boldsymbol{m}_\mathrm{e}$ and the element stiffness matrix $\boldsymbol{k}_\mathrm{e}$, which are calculated using the Gauss quadrature rule in three-dimensions with two integration points in each direction, are given as

$$\boldsymbol{m}_\mathrm{e} = \begin{bmatrix} m_0 & m_x & m_{xy} & m_y & m_z & m_{zx} & m_{xyz} & m_{yz} \\ & m_0 & m_y & m_{xy} & m_{zx} & m_z & m_{yz} & m_{xyz} \\ & & m_0 & m_x & m_{xyz} & m_{yz} & m_z & m_{zx} \\ & & & m_0 & m_{yz} & m_{xyz} & m_{zx} & m_z \\ & & & & m_0 & m_x & m_{xy} & m_y \\ & & & & & m_0 & m_y & m_{xy} \\ & & & & & & m_0 & m_x \\ & & & & & & & m_0 \end{bmatrix}, \tag{16}$$

$$\boldsymbol{k}_\mathrm{e} = \begin{bmatrix} k_0 & k_x & k_{xy} & k_y & k_z & k_{zx} & k_{xyz} & k_{yz} \\ & k_0 & k_y & k_{xy} & k_{zx} & k_z & k_{yz} & k_{xyz} \\ & & k_0 & k_x & k_{xyz} & k_{yz} & k_z & k_{zx} \\ & & & k_0 & k_{yz} & k_{xyz} & k_{zx} & k_z \\ & & & & k_0 & k_x & k_{xy} & k_y \\ & & & & & k_0 & k_y & k_{xy} \\ & & & & & & k_0 & k_x \\ & & & & & & & k_0 \end{bmatrix}. \tag{17}$$

Here, the components of matrices $\boldsymbol{m}_\mathrm{e}$ and $\boldsymbol{k}_\mathrm{e}$ are respectively given as

$$\begin{aligned} m_0 &= \frac{h^3}{64}(1+\alpha_m^2)^3, \\ m_x = m_y = m_z &= \frac{h^3}{64}(1-\alpha_m^4)(1+\alpha_m^2), \\ m_{xy} = m_{yz} = m_{zx} &= \frac{h^3}{64}(\alpha_m^2-1)^2(1+\alpha_m^2), \\ m_{xyz} &= \frac{h^3}{64}(1-\alpha_m^2)^3, \end{aligned} \tag{18}$$

and

$$
\begin{aligned}
k_0 &= \frac{3h}{16}(1+\alpha_k^2)^2, \\
k_x = k_y = k_z &= \frac{2h(1-\alpha_k^4) - h(1+\alpha_k^2)^2}{16}, \\
k_{xy} = k_{yz} = k_{zx} &= \frac{2h(\alpha_k^4-1) + h(\alpha_k^2-1)^2}{16}, \\
k_{xyz} &= -\frac{3h}{16}(1-\alpha_k^2)^2.
\end{aligned} \tag{19}
$$

The element lumped mass matrix $\boldsymbol{d}_{\mathrm{e}}$ for constructing $\boldsymbol{D}_{\mathrm{e}}$ is defined as

$$
\boldsymbol{d}_{\mathrm{e}} = \frac{h^3}{8}\begin{bmatrix}
1 & 0 & 0 & 0 & 0 & 0 & 0 & 0 \\
 & 1 & 0 & 0 & 0 & 0 & 0 & 0 \\
 & & 1 & 0 & 0 & 0 & 0 & 0 \\
 & & & 1 & 0 & 0 & 0 & 0 \\
 & & & & 1 & 0 & 0 & 0 \\
 & & & & & 1 & 0 & 0 \\
 & & & & & & 1 & 0 \\
 & & & & & & & 1
\end{bmatrix}. \tag{20}
$$

Here, only the upper triangular components are presented in the above matrices due to the symmetric matrix. By using these $\boldsymbol{m}_{\mathrm{e}}$, $\boldsymbol{k}_{\mathrm{e}}$ and $\boldsymbol{d}_{\mathrm{e}}$, the second term of Eq. (13) can be calculated as

$$
\Delta t^2 c_0^2 \boldsymbol{D}^{-1}\boldsymbol{M}\boldsymbol{D}^{-1}\boldsymbol{K}\boldsymbol{p}^n = \frac{64\Delta t^2 c_0^2}{h^6} M_c K_c \boldsymbol{p}^n_{x,y,z}, \tag{21}
$$

with

$$
\begin{aligned}
M_c =& (m_0 + m_x C_x + m_y C_y + m_z C_z + m_{xy} C_{xy} + m_{yz} C_{yz} + m_{zx} C_{zx} + m_{xyz} C_{xyz}), \\
K_c =& (k_0 + k_x C_x + k_y C_y + k_z C_z + k_{xy} C_{xy} + k_{yz} C_{yz} + k_{zx} C_{zx} + k_{xyz} C_{xyz}),
\end{aligned} \tag{22}
$$

where

$$
\begin{aligned}
C_{xy} =& C_x C_y,\ C_{yz} = C_y C_z,\ C_{zx} = C_z C_x,\ C_{xyz} = C_x C_y C_z, \\
C_x =& \cos(k_x^h h),\ C_y = \cos(k_y^h h),\ C_z = \cos(k_z^h h).
\end{aligned} \tag{23}
$$

By constructing Eq. (13) from the Eqs. (15) and (21), the dispersion relation, which represents the relation between the exact speed of sound c_0 and the

approximate speed of sound c^h, becomes

$$c_0 = \sqrt{\frac{h^6(1-\cos c^h k^h \Delta t)}{32\Delta t^2 M_c K_c}}. \tag{24}$$

Here, $k^h = \omega^h / c^h$. Using Taylor expansion with respect to k^h after substituting components of $\boldsymbol{m}_\mathrm{e}$ and $\boldsymbol{k}_\mathrm{e}$ into Eq. (24), the dispersion error can be evaluated as

$$\frac{|c_0 - c^h|}{c_0} = \frac{k^4 h^4}{1440}[B_1 + B_2 + B_3 + B_4], \tag{25}$$

where

$$\begin{aligned}
B_1 &= 8 - 10\tau^2 + 2\tau^4, \\
B_2 &= -\chi \cos^2\theta \sin^2\theta, \\
B_3 &= \chi \cos^2\phi \sin^2\phi \cos^2\theta \sin^2\theta, \\
B_4 &= -\cos^2\phi \sin^2\phi \sin^2\theta(\chi - 9\cos^2\theta \sin^2\theta), \\
\chi &= 5\tau^4 - 20\tau^2 + 19.
\end{aligned} \tag{26}$$

Using Eq. (25), the dispersion error of the explicit TD-FEM can be estimated at all directions of wave propagation for given wavenumber, with various element sizes and time intervals. Note that Eq. (25) can be reduced to the two-dimensional dispersion error equation in Ref. [15] by transforming a spherical coordinate system into a two-dimensional polar coordinate system.

3.2. Stability condition

We derive the stability condition of the explicit TD-FEM in three-dimensions following the stability analysis presented in Ref. [15], which is based on Von Neumann's stability analysis. First, we assume a relation $\boldsymbol{p}^{n+1} = A\boldsymbol{p}^n$, where A is the amplification factor. Using the equation, Eq. (13) can be defined as

$$(A - 2 + A^{-1})\boldsymbol{p}^n + B\boldsymbol{p}^n = 0, \tag{27}$$

where $B = \Delta t^2 c_0^2 \boldsymbol{D}^{-1}\boldsymbol{M}\boldsymbol{D}^{-1}\boldsymbol{K}$. After simplification, we can obtain a quadratic equation as

$$A^2 + (B-2)A + 1 = 0. \tag{28}$$

From the quadratic formula the solution is

$$A = \frac{-(B-2) \pm \sqrt{(B-2)^2 - 4}}{2}. \tag{29}$$

For stable computation $|A| \leq 1$ is necessary. This leads to $0 \leq B \leq 4$. Substituting the element components of $\boldsymbol{m}_{\mathrm{e}}$ and $\boldsymbol{k}_{\mathrm{e}}$ into B, B becomes the function of C_x, C_y, C_z and τ as presented below.

$$B = -\frac{\tau^2}{1296} C_x' C_y' C_z' [C_x C_y C_z + 3(C_x C_y + C_y C_z + C_z C_x) + 5(C_x + C_y + C_z) - 25], \tag{30}$$

where

$$\begin{aligned} C_x' &= [7 - C_x + \tau^2 (C_x - 1)], \\ C_y' &= [7 - C_y + \tau^2 (C_y - 1)], \\ C_z' &= [7 - C_z + \tau^2 (C_z - 1)]. \end{aligned} \tag{31}$$

Further, $|C_x| \leq 1$, $|C_y| \leq 1$ and $|C_z| \leq 1$ from the definitions of Eq. (23). B has the maximum value 4 at $C_x = C_y = C_z = -1$ and $\tau = 0.673988$. Thus, the stability condition of explicit TD-FEM without the dissipation term is

$$\Delta t_{\mathrm{crit}} \leq \frac{0.673988 h}{c_0}. \tag{32}$$

3.3. Comparison with implicit TD-FEM

To show the dispersion property of explicit TD-FEM, the dispersion errors at all directions of wave propagation are calculated using Eq. (25) and compared with those of two implicit TD-FEM using CAA and FG. The dispersion errors of CAA and FG are respectively calculated using Eqs (5) and (7). In those calculations, $k = 41.04$, c_0 =343.7 m/s, and $h = 0.03$ m are considered. Here, $kh = 1.2312$. To confirm the effect of time interval on the resulting accuracy, we used 10 kinds of time intervals Δt, as $\Delta t = \Delta t_{\mathrm{crit}}$, $0.9\Delta t_{\mathrm{crit}}$, $0.8\Delta t_{\mathrm{crit}}$, $0.7\Delta t_{\mathrm{crit}}$, $0.6\Delta t_{\mathrm{crit}}$, $0.5\Delta t_{\mathrm{crit}}$, $0.4\Delta t_{\mathrm{crit}}$, $0.3\Delta t_{\mathrm{crit}}$, $0.2\Delta t_{\mathrm{crit}}$ and $0.1\Delta t_{\mathrm{crit}}$. Here, Δt_{crit} is Δt at stability limit for each method. Note that we conducted the same investigation for other combinations of k and h with equal kh. Two combinations ($k = 20.52$ and $h = 0.06$ m, and $k = 82.08$ and $h = 0.015$ m) were considered. For these combinations, we obtained the same results as the case with $k = 41.04$ and $h = 0.03$ m.

Figures 3(a)–(d) present the dispersion errors of explicit TD-FEM at all wave propagation directions with $\Delta t = \Delta t_{\mathrm{crit}}$, $0.8\Delta t_{\mathrm{crit}}$, $0.6\Delta t_{\mathrm{crit}}$ and $0.4\Delta t_{\mathrm{crit}}$. The maximum dispersion errors occur at axial directions regardless of Δt values, whereas the minimum value occurs at a diagonal direction (θ,

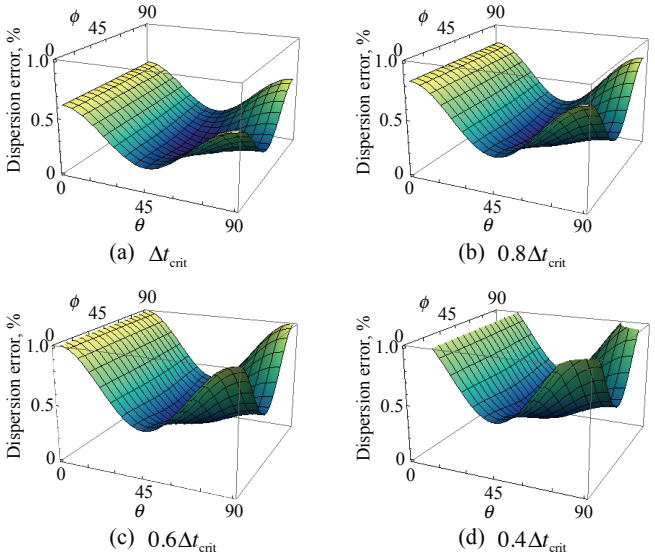

Figure 3: Comparison of dispersion error in explicit TD-FEM at all directions of wave propagation with various Δt: (a) $\Delta t = \Delta t_{\mathrm{crit}}$, (b) $\Delta t = 0.8\Delta t_{\mathrm{crit}}$, (c) $\Delta t = 0.6\Delta t_{\mathrm{crit}}$, and (d) $\Delta t = 0.4\Delta t_{\mathrm{crit}}$.

$\phi) = (55°, 45°)$. It is also confirmed that the dispersion errors become larger for smaller Δt.

Figures 4(a)–(d) present the dispersion errors of CAA at all wave propagation directions with $\Delta t = \Delta t_{\mathrm{crit}}$, $0.8\Delta t_{\mathrm{crit}}$, $0.6\Delta t_{\mathrm{crit}}$ and $0.4\Delta t_{\mathrm{crit}}$. The magnitude of dispersion error at each direction is dependent on the values of Δt. At the stability limit, the maximum dispersion error occurs at a diagonal direction $(\theta, \phi) = (55°, 45°)$, whereas the minimum errors occur at axial directions. For smaller values of Δt, the maximum and the minimum dispersion errors occur at axial directions and a diagonal direction $(\theta, \phi) = (55°, 45°)$, respectively. Note that CAA has an interesting property at $0.8\Delta t_{\mathrm{crit}}$, where the magnitude of dispersion errors at all wave propagation directions are almost the same, i.e., the error is isotopic at $0.8\Delta t_{\mathrm{crit}}$.

Figures 5(a)–(d) present the dispersion errors of FG at all wave propagation directions with $\Delta t = \Delta t_{\mathrm{crit}}$, $0.8\Delta t_{\mathrm{crit}}$, $0.6\Delta t_{\mathrm{crit}}$ and $0.4\Delta t_{\mathrm{crit}}$. Similar to the explicit TD-FEM, the maximum and minimum dispersion errors occur respectively at axial directions and at $(\theta, \phi) = (55°, 45°)$, but the magnitude is almost the same regardless of Δt values.

Figure 6 shows relationships between the mean dispersion error over prop-

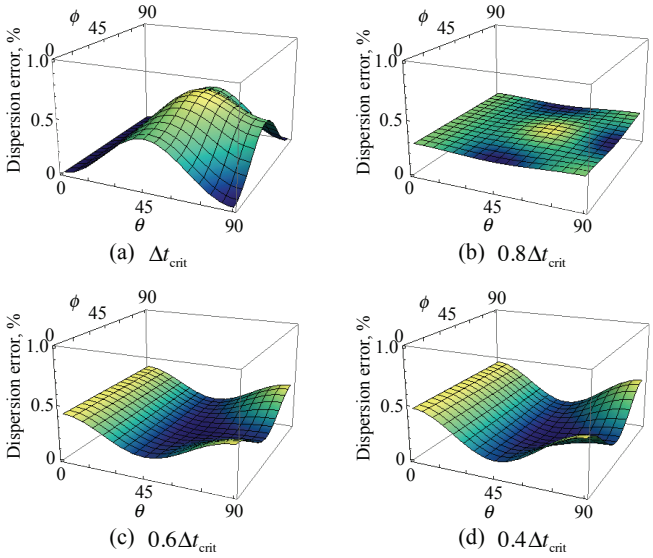

Figure 4: Comparison of dispersion error in implicit TD-FEM (CAA) at all directions of wave propagation with various Δt: (a) $\Delta t = \Delta t_{\text{crit}}$, (b) $\Delta t = 0.8\Delta t_{\text{crit}}$, (c) $\Delta t = 0.6\Delta t_{\text{crit}}$, and (d) $\Delta t = 0.4\Delta t_{\text{crit}}$.

agation angles and time interval for all methods. Clearly, Δt has the most influence on the resulting accuracy for the explicit TD-FEM. The mean dispersion error increases significantly for smaller Δt. The mean error is 0.33% at the stability limit, but the magnitude becomes 0.77% at $\Delta t = 0.1\Delta t_{\text{crit}}$. Meanwhile, the behavior of the mean dispersion errors in the two implicit methods is more stable than that of explicit method with smaller values of the error. The CAA has the maximum error at the stability limit, and the error decreases slightly for smaller Δt. The error is 0.31% at the stability limit, and 0.25% at $\Delta t = 0.1\Delta t_{\text{crit}}$. In contrast to the CAA, the FG is the most accurate at the stability limit, and the error increases slightly for smaller Δt. The error is 0.19% at the stability limit, and 0.25% at $\Delta t = 0.1\Delta t_{\text{crit}}$.

From the above theoretical evaluation of dispersion error among three methods, it can be concluded that the use of Δt near the stability limit is especially important for the accurate computation using the explicit TD-FEM, whereas the two implicit TD-FEM can use an arbitrary value of Δt with the stable behavior of the mean dispersion error.

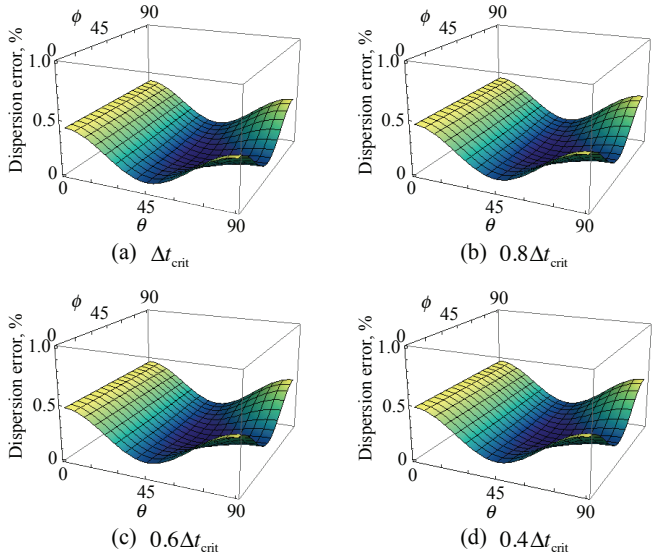

Figure 5: Comparison of dispersion error in implicit TD-FEM (FG) at all directions of wave propagation with various Δt: (a) $\Delta t = \Delta t_{\mathrm{crit}}$, (b) $\Delta t = 0.8\Delta t_{\mathrm{crit}}$, (c) $\Delta t = 0.6\Delta t_{\mathrm{crit}}$, and (d) $\Delta t = 0.4\Delta t_{\mathrm{crit}}$.

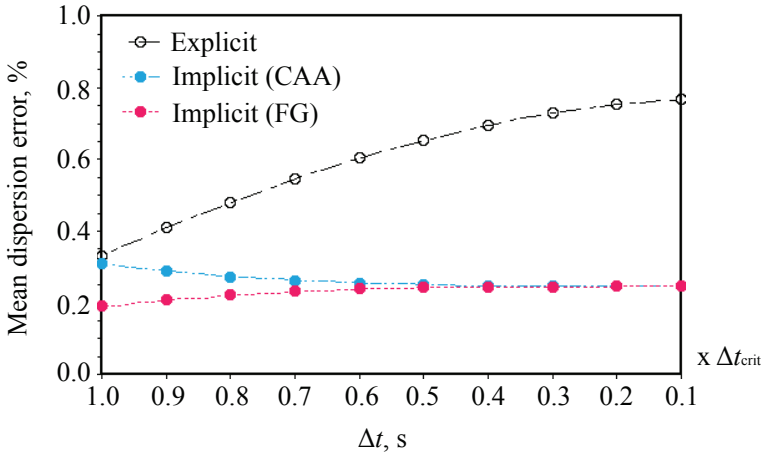

Figure 6: Comparison of mean dispersion errors over wave propagation angles for explicit TD-FEM and two implicit TD-FEM (CAA and FG).

4. Comparison with implicit TD-FEM on room acoustics simulations with an infinite impedance boundary

We performed the sound field analyses in a rectangular room with an infinite impedance boundary, to confirm the results from the theoretical analysis

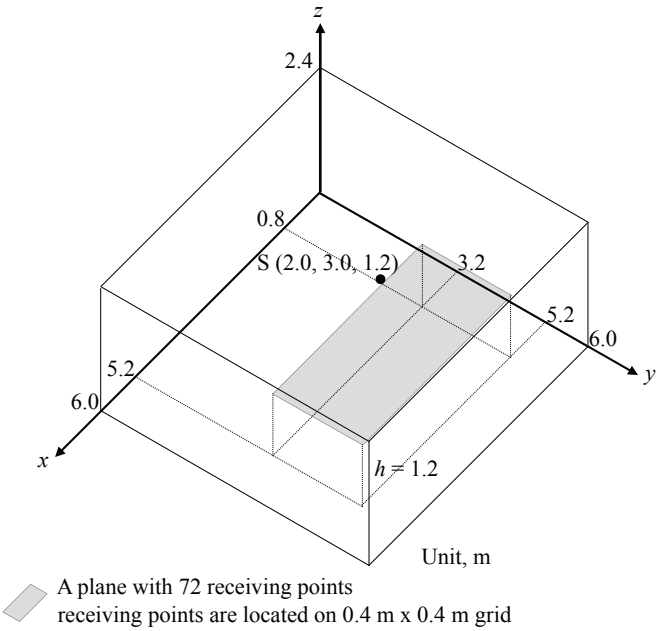

Figure 7: A rectangular room with the volume of 86.4 m^3 with a source point S and 72 receiving points. The 72 receiving points are located on a plane in gray color with 0.4 m $\times$ 0.4 m grids.

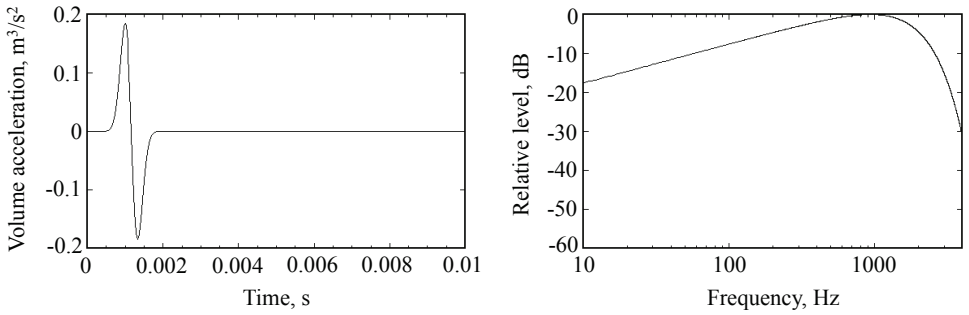

(a) Waveform (b) Frequency characteristics

Figure 8: Waveform and its frequency characteristics of sound source for numerical experiments.

in previous section and to show the efficiency and accuracy of the explicit method over the two implicit methods. The accuracy of the numerical results are shown in a comparison with the analytical solution by the method of variable separation [20]. Figure 7 shows the analyzed sound field with a source

Table 1: Specifications of FE meshes. h, λ/h, and DOF respectively represent element length, spatial resolution and degrees of freedom of FE mesh.

Mesh	h, m	λ/h	DOF
1	0.04	4.77	1,390,861
2	0.02	9.55	10,962,721
3	0.01	19.09	87,049,441

point S and receiving points, in which 72 receiving points were located on a plane with 0.4 m $\times$ 0.4 m grids. c_0 and the air density ρ_0 were respectively assumed to be 343.7 m/s and 1.205 kg/m^3. The sound source used here is a modulated Gaussian pulse [11]. The waveform and its frequency characteristics are shown in Fig. 8. Here, the upper limit of frequency was assumed as 1.8 kHz. We calculated sound pressures at the 72 receiving points up to 200 ms. In first numerical experiments, we confirm the results in previous section especially focusing on the effect of time interval on the resulting accuracy. Then, we show the efficiency and accuracy of the explicit method over the two implicit methods using three configurations of FE meshes with different spatial resolutions. Table 1 lists the FE meshes used, element length h, the spatial resolution of FE mesh λ/h, and the degrees of freedom of FE mesh, where λ represents the wavelength at upper limit frequency. The convergence tolerance for the stopping criterion of CG method was set to 10^{-6} for the implicit TD-FEM. The diagonal scaling was used as a preconditioning of the CG method.

4.1. Effect of time intervals on the resulting accuracy

To show the effect of Δt on the resulting accuracy in the three methods, the sound field in the rectangular room was analyzed using Mesh 1 in Table 1 with various Δt's. The Δt's were respectively set to Δt_{crit}, $0.8\Delta t_{\text{crit}}$, $0.6\Delta t_{\text{crit}}$, and $0.4\Delta t_{\text{crit}}$. A relative error in sound pressure between the analytical method and FE analysis was used to evaluate the accuracy quantitatively, which is given as

$$e_p = \frac{1}{N_{\text{step}}} \sum_{j=1}^{N_{\text{step}}} e(t_j), \tag{33}$$

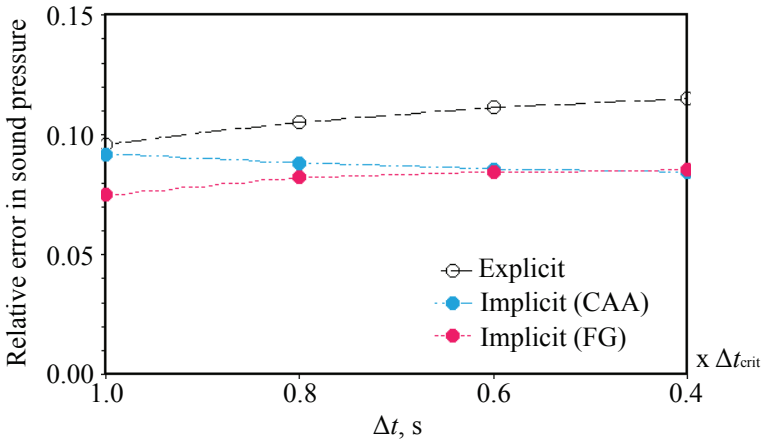

Figure 9: Comparison of relative errors in sound pressure among explicit TD-FEM and implicit TD-FEM using CAA and FG.

with

$$e(t) = \sqrt{\frac{1}{N}\frac{\sum_{i=1}^{N}[p_{\text{Ana.}}(\boldsymbol{x}_i,t) - p_{\text{FEM}}(\boldsymbol{x}_i,t)]^2}{\sum_{i=1}^{N} p_{\text{Ana.}}(\boldsymbol{x}_i,t)^2}}, \tag{34}$$

where N_{step} represents the number of time steps. $p_{\text{Ana.}}(\boldsymbol{x}_i,t)$ and $p_{\text{FEM}}(\boldsymbol{x}_i,t)$ represent sound pressures at receiving point $\boldsymbol{x}_i$ at time t calculated using the analytical method and TD-FEM, respectively. Figure 9 shows a comparison of the relative errors among the explicit TD-FEM and the implicit TD-FEM using CAA and FG. Cleary, the numerical results follow those of the theoretical results in previous section. The Δt has the most influence on the accuracy of the explicit TD-FEM, and the relative error e_p increases for smaller Δt. Meanwhile, the influence of Δt value on the resulting accuracy of two implicit methods is smaller than that of the explicit method.

4.2. Computational efficiency

To show the computational efficiency of the explicit TD-FEM over the two implicit TD-FEM, the sound field in the rectangular room was again analyzed using Mesh 1∼3 in Table 1, which have different spatial resolutions. Total number of sparse matrix-vector products (SMVP), which is the main numerical operation of the explicit and implicit methods, was used to evaluate the numerical efficiency of the method, instead of the computational time. The accuracy was also evaluated using Eq. (33). The Δt's were respectively set to the critical values for each method.

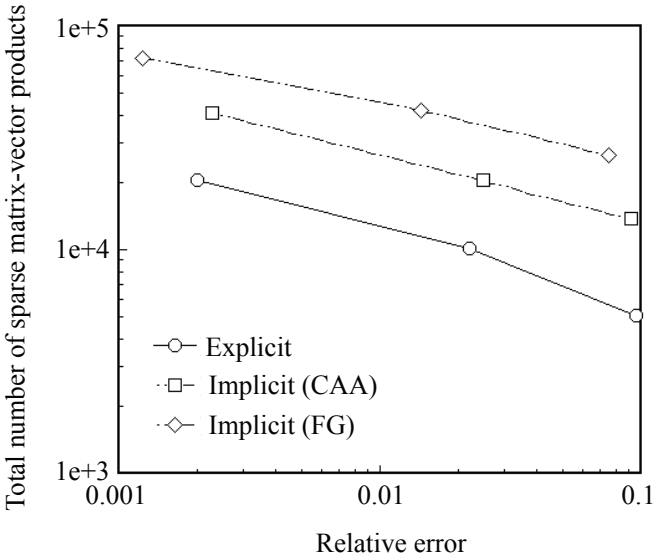

Figure 10: Relationship between the total numbers of SMVP and the relative errors among explicit TD-FEM and implicit TD-FEM using CAA and FG.

Figure 10 shows the relationship between the total numbers of SMVP and the relative errors among three TD-FEM. The explicit TD-FEM requires less computational effort than the two implicit methods to obtain the same accurate results. Meanwhile, one of the implicit methods is computationally more efficient than the explicit method in term of the memory requirement to obtain the same accurate results, as shown in Fig. 11. From the results of this section, we conclude that the explicit TD-FEM with Δt_{crit} is computationally more efficient than the implicit methods in term of the computational time in room acoustics simulations with an infinite impedance boundary.

5. Stability condition in the case with a finite impedance boundary

To examine the numerical stability of explicit TD-FEM on room acoustics simulations with a finite impedance boundary, we conducted numerical experiments with various impedance conditions. The sound field in a cubic room of 1 m^3 was analyzed in the following three conditions (Fig. 12): (a) Cond. 1: One surface has a finite impedance and the remaining surfaces have the infinite impedance, (b) Cond. 2: Adjacent two surfaces have a finite impedance and the remaining surfaces have the infinite impedance, and

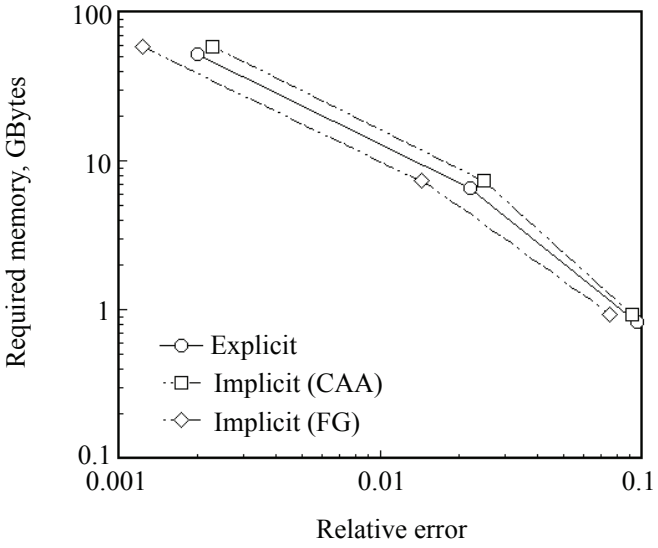

Figure 11: Relationship between the required memory and the relative errors among explicit TD-FEM and implicit TD-FEM using CAA and FG.

(c) Cond. 3: Three surfaces have a finite impedance, in which two edges of the surfaces are connected with other absorbing surfaces each other, and the remaining surfaces have the infinite impedance. These conditions were designed for examining the stability of scheme at a node on the plane, edge and corner. Six normalized impedance ratio's (z_{n}'s) with different degrees of absorption were systematically given for the finite impedance surface, which are $z_{\mathrm{n}} = 32.56$, 13.44, 7.14, 3.87, 2.597 and 1.0. These z_{n}'s respectively correspond to the statistical absorption coefficient, α_{s}, of 0.20, 0.40, 0.60, 0.80, 0.90 and 0.91 according to Paris's formula. The upper-limit frequency of the analysis is 1800 Hz, and sound pressure up to 1.0 s was calculated with various time intervals to examine the stability of scheme. The time intervals were set to $\Delta t = m\Delta t_{\mathrm{crit}}$, in which m was systematically set to 0.95∼0.25 with 0.05 step. The element size of FE mesh is 0.025 m.

Table 2 lists the maximum values of m for stable computations obtained from the numerical analysis. The stability of scheme becomes worse for smaller z_{n} and with increasing the absorbing surfaces. These results indicate that the stability of the explicit TD-FEM is dependent on the impedance values of boundaries, and the node on the corner has the hardest stability condition because the stability of Cond. 3 is the worst. Considering the

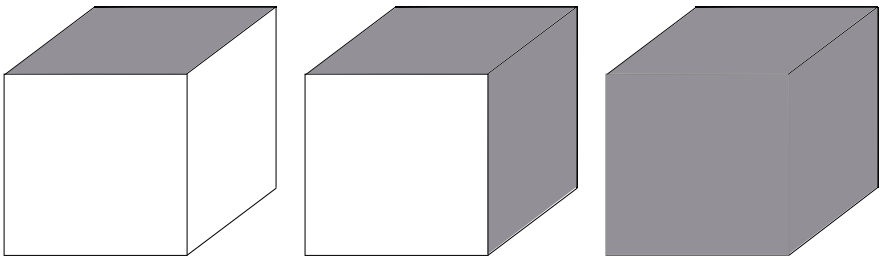

(a) Cond. 1 (b) Cond. 2 (c) Cond. 3

Figure 12: Absorption conditions of surfaces for the numerical stability analysis. Surfaces in gray color have a finite impedance value.

Table 2: The maximum value of m for stable computation.

	z_{n} (α_{s})					
Cond.	32.56 (0.2)	13.44 (0.4)	7.14 (0.6)	3.87 (0.8)	2.597 (0.9)	1.0 (0.91)
1	0.95	0.95	0.90	0.85	0.75	0.50
2	0.95	0.95	0.85	0.75	0.65	0.35
3	0.95	0.90	0.80	0.65	0.55	0.25

results in the case with an infinite impedance boundary, the explicit TD-FEM might be effective for room acoustics simulations with moderate absorption up to $z_{\mathrm{n}} = 7.140$ at boundaries. For this condition the use of $\Delta t = 0.8\Delta t_{\mathrm{crit}}$ is possible as shown in Cond. 3 of Table 2, which is not so hard. In addition, when the only one surface has high absorption, the use of $\Delta t = 0.85\Delta t_{\mathrm{crit}}$ is possible up to $z_{\mathrm{n}} = 3.870$ as shown in Cond. 1 of Table 2. In actual rooms, some rooms such as a classroom and a office typically have only a high absorption surface and the remaining boundaries are reflective. The present explicit TD-FEM might be useful for the sound field analysis of these rooms. This point is further investigated by comparison with the implicit methods in the next section. Meanwhile the scheme is not effective for higher absorption conditions with smaller impedance values at boundaries. For the conditions the use of smaller time interval is necessary, but the dispersion error at nodes in the room increases significantly as shown in the results from the theoretical analysis. Thus, the use of implicit TD-FEM is recommended for the higher absorbing conditions.

6. Comparison with implicit TD-FEM on room acoustics simulations with a finite impedance boundary

The sound field in a rectangular room (Fig. 7) was analyzed with a frequency-independent finite impedance boundary, to show the efficiency and accuracy of the explicit method over the two implicit methods in the case with absorbing conditions. Note that the investigation was limited to the case with less-restricted stability condition for the explicit method, based on the results in previous section. We assumed two absorbing conditions for the boundary surfaces: (a) Cond. 4: the ceiling has $z_{\mathrm{n}} = 13.44$ ($\alpha_{\mathrm{s}} = 0.4$) and the remaining boundaries have $z_{\mathrm{n}} = 71.519$ ($\alpha_{\mathrm{s}} = 0.1$), and (b) Cond. 5: the ceiling has $z_{\mathrm{n}} = 3.87$ ($\alpha_{\mathrm{s}} = 0.8$) and the remaining boundaries have $z_{\mathrm{n}} = 71.519$ ($\alpha_{\mathrm{s}} = 0.1$). The sound pressure was respectively calculated up to 0.53 s and 0.36 s for each condition, which correspond to the reverberation times calculated by Eyring formula. The sound source used here is the same as that shown in Fig. 8. Also, Meshes 1$\sim$3 in Table 1 were used for the investigation. Regarding the stability of the explicit TD-FEM for each condition, we again conducted the numerical stability analysis. As the results, we use $\Delta t = 0.90\Delta t_{\mathrm{crit}}$ and $\Delta t = 0.85\Delta t_{\mathrm{crit}}$ for Cond. 4 and Cond. 5, respectively. Note that the stability is not so hard if absorption coefficients of the remaining boundaries are up to 0.4. In this case, $\Delta t = 0.80\Delta t_{\mathrm{crit}}$ can be used. For the two implicit TD-FEM the Δt's were respectively set to their critical values. The accuracy was evaluated by the relative error in Eq. (33), in which a reference solution was used instead of the analytical solution. The reference solution was calculated by the most accurate implicit TD-FEM with FG, using Mesh 3 which is the finest mesh.

Figure 13(a) and (b) show the relationship between the total numbers of SMVP and the relative errors among three TD-FEM for Cond. 4 and Cond. 5. For both conditions the explicit TD-FEM is computationally more efficient than the implicit methods to obtain the same accurate results, with less total numbers of SMVP. Figure 14(a) and (b) show the relationship between memory requirements and the relative errors among three TD-FEM for Cond. 4 and Cond. 5. The explicit method requires larger memory than the implicit methods to obtain the same accurate results. From these results, we can conclude that the explicit TD-FEM is effective than the implicit TD-FEM in term of computational time for room acoustics simulations with larger impedance values at boundaries because Δt near the stability limit can be used.

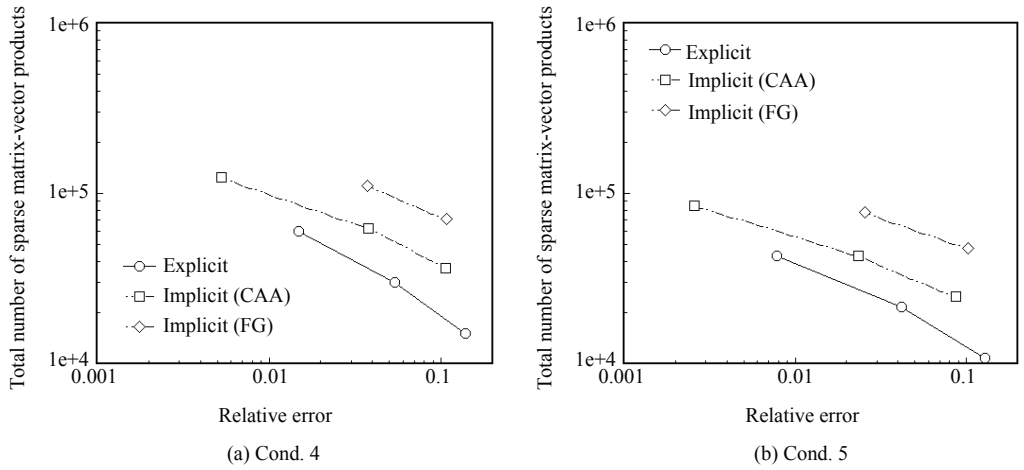

Figure 13: Relationship between the total numbers of SMVP and the relative errors among explicit TD-FEM and implicit TD-FEM using CAA and FG: (a) Cond. 4 and (b) Cond. 5.

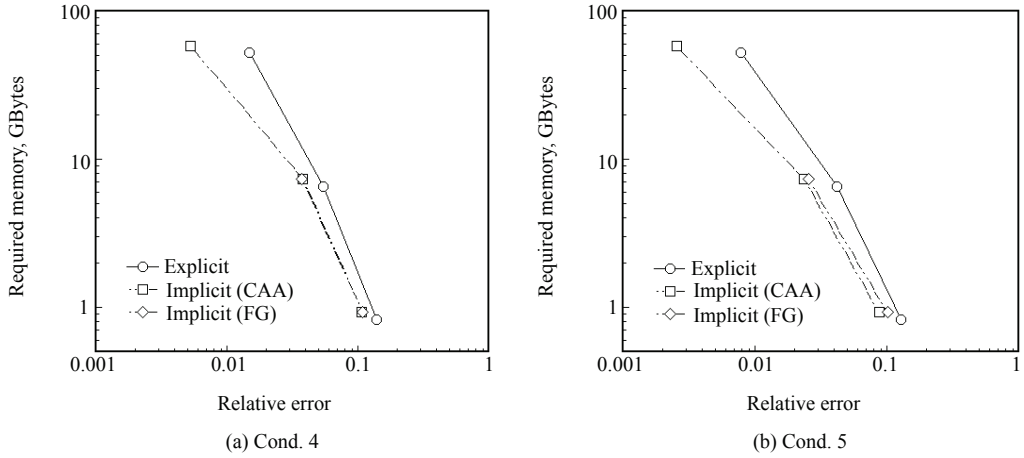

Figure 14: Relationship between the memory requirements and the relative errors among explicit TD-FEM and implicit TD-FEM using CAA and FG: (a) Cond. 4 and (b) Cond. 5.

7. Conclusions

In this paper, the performance of the explicit TD-FEM using MIR on room acoustics simulations with a frequency-independent finite impedance boundary have been demonstrated by comparison with the two implicit TD-

FEM using MIR. The three-dimensional dispersion error analysis revealed that the accuracy of explicit TD-FEM is dependent on the value of time interval. This method is the most accurate at the stability limit, and the accuracy becomes worse with the use of smaller time interval. Meanwhile, for the implicit TD-FEM using CAA and FG the influence of time interval on the resulting accuracy is not significant. These results were also confirmed by the numerical experiments, in which the sound field in a rectangular room with an infinite impedance boundary was analyzed. Numerical stability analysis for the room acoustics simulation with a finite impedance boundary revealed that the stability of this explicit TD-FEM is dependent on the impedance values at boundary surfaces, and the stability becomes worse for smaller impedance values. Numerical experiments indicated that the explicit TD-FEM is computationally more efficient than the implicit TD-FEM in term of computational time for acoustics simulations of a room with larger impedance values at boundaries and with cubic FEs. The development of improved method is now undergoing.

Acknowledgment

This work was in part supported by JSPS KAKENHI Grant Number 15K18167. The computation was partly carried out using the computer facilities at Research Institute for Information Technology, Kyushu University.

References

[1] Sakuma T, Sakamoto S, Otsuru T, Computational simulation in architectural and environmental acoustics-Methods and applications of wave-based computation, Springer; 2014.

[2] LL Thompson, A review of finite-element methods for time-harmonic acoustics, J Acoust Soc Am 2006; 119(3):1315–30.

[3] Marburg S, Nolte B, Computational acoustics of noise propagation in fluids-finite and boundary element methods, Springer; 2008.

[4] Saad Y, Iterative methods for sparse linear systems, Second edition, SIAM; 2003.

[5] Okuzono T, Otsuru T, Tomiku R, Okamoto N, A finite-element method using dispersion reduced spline elements for room acoustics simulation, Appl Acoust 2014;79:1–8.

[6] Choi S, Tachibana H, Estimation of impulse response in a room by the finite element method, J Acoust Soc Jpn 1993; 49(5):328–33.(in Japanese)

[7] Otsuru T, Fujii K, Finite elemental analysis of sound field in rooms with sound absorbing materials, Proc Inter-noise 1994; 94:2011–4.

[8] Easwaran V, Craggs A, Transient response of lightly damped rooms: a finite element approach, J Acoust Soc Am 1996; 99(1):108–13.

[9] Easwaran V, Craggs A, An application of acoustic finite element models to finding the reverberation times of irregular rooms, Acoust Acta Acoust 1996; 82:54–64.

[10] Okuzono T, Otsuru T, Tomiku R, Okamoto N, Fundamental accuracy of time domain finite element method for sound-field analysis of rooms, Appl Acoust 2010;71(10):940–6.

[11] Okuzono T, Otsuru T, Tomiku R, Okamoto N, Application of modified integration rule to time-domain finite-element acoustic simulation of rooms, J Acoust Soc Am 2012;132(2):804–13.

[12] Otsuru T, Okuzono T, Tomiku R, Asniawaty K, Large-scale finite element sound field analysis of rooms using a practical boundary modeling technique, In: Proc 19th international congress on sound and vibration 2012 on CD-ROM(No.632);2012.

[13] Otsuru T, Tomiku R, Basic characteristics and accuracy of acoustic element using spline function in finite element sound field analysis, Acoust Sci Technol 2000; 21(2):87–95.

[14] Okuzono T, Otsuru T, Tomiku R, Okamoto N, Minokuchi T, Speedup of time domain finite element sound field analysis of rooms, Proc Inter-noise 2008 on CD-ROM(0877); 2008.

[15] Yue B, Guddati MN, Dispersion-reducing finite elements for transient acoustics, J Acoust Soc Am 2005; 118(4):2132–41.

[16] Okuzono T, Otsuru T, Sakagami K, Applicability of an explicit time-domain finite-element method on room acoustics simulation, Acoust Sci Technol 2015; 36(4):377–380.

[17] Newmark NM, A method of computation for structural dynamics, J Eng Mech Div 1959; 85:67–94.

[18] Hughes TJR, The finite element method linear static and dynamic finite element analysis, Dover; 2000.

[19] Krenk S, Dispersion-corrected explicit integration of the wave equation, Comput Methods Appl Mech Engrg 2001; 191:975–87.

[20] Sakamoto S, Phase-error analysis of high-order finite difference time-domain scheme and its influence on calculation results of impulse response in closed sound field, Acoust Sci Technol 2007; 28(5):295–309.